

Search for spectroscopic binaries using rotational velocities in five open clusters observed by ESO.

Mikhail Kovalev,^{1,2,3,4} ★ Mariyam Ahmed,⁵Randa Asa'd,⁵ †

¹*Yunnan Observatories, China Academy of Sciences, Kunming 650216, China*

²*Key Laboratory for the Structure and Evolution of Celestial Objects, Chinese Academy of Sciences, Kunming 650011, China*

³*Sternberg Astronomical Institute, Leninskie Gory, Moscow 119992, Russia*

⁴*International Centre of Supernovae, Yunnan Key Laboratory, Kunming 650216, China*

⁵*Physics Department, American University of Sharjah, PO Box 26666, Sharjah, UAE*

Accepted XXX. Received YYY; in original form ZZZ

ABSTRACT

In this paper we detect double-lined spectroscopic binaries (SB2) in five open clusters: NGC 2243, NGC 2420, NGC 3532, NGC 6253 and NGC 6705 (M 11) using a method based on high values of the projected rotational velocity when they are fitted with single star spectral model. Observed spectra were obtained from ESO archive. The method was validated on sets of synthetic spectra for the single and binary stars. It is able to reliably select spectroscopic binaries without confusing them with single stars, if components in binary rotate slowly and radial velocity separation is sufficiently high. We found 60 SB2 candidates: two in NGC 2243, eight in NGC 2420 and NGC 3532, 17 in NGC 6253 and 25 in NGC 6705. Comparison with literature confirms 18 of them, thus we found 42 new SB2 candidates.

Key words: binaries: spectroscopic

1 INTRODUCTION

Binary systems are a major area of astronomical study for several reasons. Approximately 40% of stars in the Milky Way are part of a binary or higher-order system (Moe & Stefano 2017). Unidentified binary spectra are also potentially responsible for errors in atmospheric parameter estimation performed by data processing pipelines associated with spectroscopic surveys, thus cataloguing binaries can improve the accuracy of these estimations (Schlesinger et al. 2010; El-Badry et al. 2018a). In addition to being a direct method of estimating stellar masses by using relations derived from Kepler’s laws (Serenelli et al. 2021), detecting binary systems and studying their orbital elements allows us to constrain models of stellar evolution. Spectra from binary stars can be used to determine the properties of each star in the system, such as its mass, size, temperature, and luminosity. This information can then be used to gain insight into the processes that govern the formation and evolution of stars. How the stars in a binary system interact with each other, exchange mass, and evolve over time can be understood by observing binary systems at different stages of their evolution. This observation can provide important clues about the processes that govern the evolution of stars and the formation of new stars.

Binary systems are of three main types, mainly divided by the method used to observe and study their components and dynamics. A visual binary is one that can be resolved by telescopes into two separate objects. Such binaries provide the advantage of allowing the measurement of all orbital elements associated with it, since their orbits

can be traced by observing the stars’ movement over time (Piccotti et al. 2020). However, the detection of visual binaries is subject to the limitation of distance as it is constrained by the angular resolution of the instrument used. The second group of binary stars are eclipsing binaries, where the orbit of the system is edge-on to the line of sight. These binaries are instead studied by measuring the dip in flux that occurs when one component passes in front of or behind the other. Finally, the third kind of binaries are spectroscopic binaries (SB). These stars are too close together to be resolved as distinct objects and thus appear as one star. Despite it being not possible to resolve the two components, the presence of second star can be inferred from peculiarities in the spectra recorded from the system. The spectra of an SB system also reveal the stars’ motion relative to one another. As the two stars orbit each other, they periodically reach points in their orbit when they are moving away from or towards Earth. However, because the orbit of the system is not always perpendicular to us, we only observe the effect of the component of the movement that is in our direction. Consequently, when some component of their orbital velocities is in our line-of-sight, their observed spectral lines shift back and forth due to the Doppler effect. SB systems are particularly useful for studying the properties of binary stars, as they provide an opportunity to observe the properties of two stars over much longer distances than visual binaries. This fact allows SB systems to even be detected in even other nearby galaxies (Merle et al. 2020). These three categories are not mutually exclusive; eclipsing binaries are special cases of visual or, most commonly, spectroscopic binaries. SBs are further classified by the number of spectral components, such as spectral lines, that are visible in their spectra (SB_n, where $n \geq 1$). In SB1 stars, the spectrum of one star dominates the other due to the primary star being much brighter, and only one spectrum

★ E-mail: mikhail.kovalev@ynao.ac.cn

† E-mail: raasad@aus.edu

is visible. These star systems are classified as binaries by detecting periodic shifts in the radial velocity of the primary component that cannot be explained by other reasons such as pulsations. The detection of SB2s is simpler since the spectral components of both stars are clearly visible when a component of their orbital movement is in our line-of-sight. The consequent Doppler shift of each of their spectra causes a separation of their measured radial velocities. SB2s with non-zero radial velocity separation of components are usually detected by analysis using cross-correlation functions (CCF) and detecting of multiple peaks in the CCF (Merle et al. 2017). In contrast, machine-learning algorithms are also able to detect SB2s with $|\Delta RV|$ close to zero by fitting the observed spectrum to composite spectral models (El-Badry et al. 2018a,b; Kovalev & Straumit 2022).

However detecting SB2 is not straight forward, as composite spectral model may not be picking up the contribution of a secondary star, but may just be fitting to the spectral noise. To further improve selection criteria to reliably detect SB2 candidates we can use projected rotational velocity ($V \sin i$). This is the speed at which star rotates around it's axis. Stellar rotation is one factor that can cause the broadening of spectral lines, another being the presence of a binary system where the two spectral components are too close to be resolved separately. Kovalev et al. (2022b) used a new selection criterion to find SB2s from spectral analysis, which involves the projected rotational velocity estimated for the single and binary spectral fit. Thus, this selection criteria works under the principle of separating rapidly rotating single stars, with broad spectral components, from two slowly rotating stars in a binary system. Kovalev et al. (2022b) tested this new method on observations from the NGC 6705 (M11) cluster and LAMOST-MRS data (Liu et al. 2020).

The current paper aims to validate this selection method on five different open clusters NGC 2243, NGC 2420, NGC 3532, NGC 6253 and NGC 6705. These clusters vary significantly in both age and metallicity, so they are good test subjects to validate the reliability of the method.

2 DATA

In this study we arbitrary select five open star clusters in the European Southern Observatory (ESO) archive to realistically detect SB2 stars. The spectra in all clusters were obtained with the VLT (Very Large Telescope)/GIRAFFE spectrograph (Pasquini et al. 2002) using the HR15N setup, which spans 380 Å, from 6440 Å to 6820 Å, at a resolution of $R = \lambda/\Delta\lambda \approx 19200$. This setting includes the $H\alpha$ line, a deep spectral line of the hydrogen atom with a wavelength of approximately 6563 Å, to allow for easier distinction between the two spectral components of SB2s. Additionally there are more spectral observations in HR15N setting than in others (Randich et al. 2022).

The selected clusters are listed in Table 1, which listed literature age and metallicities together with the number of available spectra selected inside one degree cone. All spectra are publicly available in ESO portal¹ and were observed as a part of Gaia-ESO survey (Gilmore et al. 2012), except for NGC 6253 which was observed earlier. Each target has only one observation in HR15N setting. We use all available spectra and did not check their membership for each cluster.

open cluster	log Age, yrs	[Fe/H], dex	N_{spectra}
NGC 2243	9.64	-0.45 ± 0.05	640
NGC 2420	9.24	-0.15 ± 0.02	542
NGC 3532	8.6	-0.03 ± 0.08	906
NGC 6253	9.54	0.30	202
NGC 6705 (M 11)	8.49	0.03 ± 0.05	1025

Table 1. The list of selected open clusters. Ages and metallicities are from Randich et al. (2022), except for NGC 6253 with values from de Marchi et al. (2010).

3 METHOD

We use the method introduced in Kovalev et al. (2022b) to detect SB2 stars. The observed spectra are fit to a single star and binary system synthetic model, and the associated goodness-of-fit measure, the reduced χ^2 score, is estimated for both.

$$\chi^2 = \frac{1}{N-p} \sum_{\lambda=\lambda_{min}}^{\lambda=\lambda_{max}} \left[\frac{f_{\lambda,obs} - f_{\lambda,model}}{\sigma_{\lambda}} \right]^2 \quad (1)$$

where $N = 7441$ is the number of wavelength points in the HR15N observation, p is the number of estimated parameters for a single star or binary model, and σ_{λ} is the uncertainty (error) of the observed flux. Each model is also multiplied by a linear combination of first four Chebyshev polynomials, which is used for normalisation, similarly to Kovalev et al. (2022b). We used simple linear interpolation² in the grid of 1083 spectral models, computed using NLTE MPIA spectral synthesis interface³ (see Chapter 4 in Kovalev 2019, for details) to generate single-star stellar model, using SIU radiative transfer code by Reetz (1999). We used MAFAGS-OS atmospheric models (Grupp 2004a,b). The grid parameters include the effective temperature (T_{eff}), surface gravity ($\log(g)$), metallicity ([Fe/H]) and projected rotational velocity ($V \sin i$) randomly selected within the following ranges $T_{\text{eff}} = 5080, 8720$ K, $\log(g) = 2.9, 4.7$ cgs, $[\text{Fe}/\text{H}] = -0.46, 0.45$ dex and $(V \sin i) = 5, 290$ km s⁻¹. These ranges were selected to insure stable work of the linear interpolation. Microturbulence was set to $V_{\text{mic}} = 2$ km s⁻¹ for all models, for simplicity. We also fit for a radial velocity, therefore single star model is characterised by $p = 9$ parameters.

For the binary system model, the composite spectrum is generated by summing two single star spectral models which are scaled according to the relative luminosities of each star. The luminosity of a star is a function of its effective temperature and stellar size.

The flux of the binary model is thus given by

$$f_{\lambda,binary} = \frac{f_{\lambda,1} + k_{\lambda} f_{\lambda,2}}{(1 + k_{\lambda})}, \quad k_{\lambda} = \frac{B_{\lambda}(T_{\text{eff}1})M_1}{B_{\lambda}(T_{\text{eff}2})M_2} (\log(g)_2 - \log(g)_1) \quad (2)$$

where k_{λ} is the luminosity ratio of the two binary stars per wavelength unit, computed using black body radiation $B_{\lambda}(T_{\text{eff}})$ (Planck formula) and ratio of radii, derived using mass ratio and surface gravities. Mass ratio $q = M_1/M_2$ is fitted in the range $q = 0.1, 10$. Metallicity is fixed to the same value for both components. We also fit for radial velocities of both components, therefore binary star model is characterised by $p = 14$ parameters.

Once the observation is fitted to both single and binary models,

¹ http://archive.eso.org/wdb/wdb/adp/phase3_spectral/form

² with `SCIPY.INTERPOLATE.LINEARNDINTERPOLATE`

³ <https://nlte.mpia.de>

the improvement factor, imp , is calculated to compare both fits:

$$\text{imp} = \frac{\sum_{\lambda=\lambda_{\min}}^{\lambda_{\max}} (|f_{\lambda,\text{single}} - f_{\lambda,\text{obs}}| - |f_{\lambda,\text{binary}} - f_{\lambda,\text{obs}}|) / \sigma_{\lambda}}{\sum_{\lambda=\lambda_{\min}}^{\lambda_{\max}} (f_{\lambda,\text{single}} - f_{\lambda,\text{binary}}) / \sigma_{\lambda}} \quad (3)$$

where σ_{λ} is the uncertainty (error) associated with the observed flux. The improvement factor estimates how much the binary model improves the fit compared to the single model.

4 SELECTION CRITERIA

Binary candidates are selected using the empirical criterion from (Kovalev et al. 2022b):

$$(V \sin i)_1 + (V \sin i)_2 + (V \sin i)_{\min} < (V \sin i)_0 \quad (4)$$

where $(V \sin i)$ represents the projected rotational velocity, with subscripts 0, 1, 2 for the single star model, the primary/secondary components of the binary model, respectively and $(V \sin i)_{\min}$ takes to account possible uncertainty in measurements. This selection criterion is a new method proposed by Kovalev et al. (2022b) for selecting SB2s and was inspired by the degeneracy between $|\text{RV}_1 - \text{RV}_2|$ and $(V \sin i)_0$ of SB2s. The rationale for this criterion can be understood by considering the possibility of fitting a true single star with a binary model and vice versa:

(i) Fitting a true single star with binary model: the first possibility is the binary model selected will consist of two spectra with minimal RV separation, resembling twin stars. Thus, the estimated rotational velocities $(V \sin i)_{1,2} \sim (V \sin i)_0$, or $2(V \sin i)_0 = (V \sin i)_1 + (V \sin i)_2$. It is thus evident that most single stars will follow this relationship. On the other hand, it is possible that the primary component will fit the observed spectra very well, being identical to the single model, while the secondary component has a negligible contribution, with any value of $(V \sin i)_2$ from available range. In the second case, the improvement factor will be small and thus these fits can be filtered out easily.

(ii) Fitting a true binary system with a single star model: the single model will broaden its spectral lines to compensate for multiplicity in the spectrum by increasing a rotational velocity value. Thus, by using the selection criteria $(V \sin i)_1 + (V \sin i)_2 < (V \sin i)_0$, SB2 candidates become easy to detect as they will likely be fitted with a large value of $(V \sin i)_0$.

Additionally, to filter out specious binary fits, criterion involving the improvement factor $\text{imp} > 0.1$ is used, following Kovalev & Straumit (2022). This ensures that the binary model produces a significantly better fit to the observed spectra in comparison with the single star model. However we should note that our criteria will not select SB2s with fast rotating components if the difference $|\text{RV}_1 - \text{RV}_2|$ is small, because in this case $(V \sin i)_1 + (V \sin i)_2 > (V \sin i)_0$.

5 VALIDATION OF CRITERIA USING SYNTHETIC STARS

To validate these selection criteria two equal sets of 1000 mock single stars and 1000 mock binaries were created and used to apply the fitting technique and test the selection criteria for each cluster. Mock stars were created by selecting random points from the PAR-SEC (Bressan et al. 2012) isochrone, which represent the positions of cluster's stars on the Hertzsprung-Russell with the same age but various masses. The isochrones are computed using the cluster ages and metallicities from Table 1. The parameters used from the isochrone

are mass, effective temperature, and surface gravity, which were selected within the ranges of the grid of synthetic spectral models. For mock binaries, values for RV_1 and $(V \sin i)_{1,2}$ are randomly selected from uniform distributions: $U(\gamma - 100, \gamma + 100)$ km s⁻¹ and $U(5, 150)$ km s⁻¹ respectively, where γ is the systemic velocity of the cluster. RV_2 values are calculated using the formula:

$$\text{RV}_2 = \gamma(1 + q) - q\text{RV}_1 \quad (5)$$

where the mass ratio was computed using masses from the isochrone.

Mock single stars were generated by assigning the same values for both components for all parameters listed above, with $\text{RV}_0 = U(\gamma - 10, \gamma + 10)$ km s⁻¹ and $(V \sin i)_0$ is randomly selected from the $U(5, 150)$ km s⁻¹ distribution.

Figures 1,2 display the results of the synthetic run. Solid lines represent the functions $(V \sin i)_1 + (V \sin i)_2 = (V \sin i)_0$ (blue) and $(V \sin i)_1 + (V \sin i)_2 = 2(V \sin i)_0$ (red). Blue dotted line shows the relation $(V \sin i)_1 + (V \sin i)_2 + 5 = (V \sin i)_0$. The value $(V \sin i)_{\min} = 5$ km s⁻¹ was set to prevent the selection of single stars, based of comparison between fitted and true values, where $\sigma(\Delta(V \sin i)_0) < 2.5$ km s⁻¹ for all clusters. The open triangles represent the stars that were selected by the criteria. Effective selection of binaries by the criteria would result in no false positives, i.e. no single stars would be selected as binaries. It is apparent that no synthetic single stars (orange) appear below the blue dotted line and they strongly follow the relation $(V \sin i)_1 + (V \sin i)_2 = 2(V \sin i)_0$ for reasons described in the previous section. Another overdensities formed by the single stars are visible slightly above the relation $(V \sin i)_1 + (V \sin i)_2 = (V \sin i)_0$ for clusters NGC 2243, NGC 2420, NGC 3532 and NGC 6705. There we have single stars well fitted by the primary component, with negligible contribution from the secondary, which has small $(V \sin i)_2$. Only for young cluster NGC 3532 some single stars appear below the blue line, but usage of $(V \sin i)_{\min} = 5$ km s⁻¹ filters them out.

These findings on mock stars demonstrate the reliability of this selection method for a given clusters. From the 1000 mock binaries in each cluster, the method is able to select 219, 291, 136, 191 and 155 for NGC 2243, NGC 2420, NGC 3532, NGC 6253 and NGC 6705 respectively. Although this indicates a relatively low success rate of 13-29%, it reliably selects SB2 candidates without producing false positives; hence, the strength of this method lies in the purity of its selection, not in completeness. Notice that success rate is smaller for younger clusters with higher [Fe/H].

Fitted parameters have good agreement with true parameters for a single star model, while for the binary model it can be worse. Usually it depends on radial velocity difference between the binary components and their contribution in total light (Kovalev & Straumit 2022). However we should note that for SB2 candidate identification purpose it not absolutely necessary to get exact parameters of both components with binary model, usually it is enough to see that binary model can fit spectrum much better than the single star model. Thus we can say that in our case binary model serves as a flexible "composite spectrum template". To get more accurate estimation of the system's parameters one needs to fix mass ratio using some additional information (Kovalev & Straumit 2022) or to use simultaneous fitting of several spectra, see Kovalev et al. (2022a, 2023) for details.

6 RESULTS AND DISCUSSION

We carefully inspected all resulting spectral fits by eye and found, that spectra with signal-to-noise ratio (S/N) $S/N < 15$ are too noisy

to make reliable selection. Additionally we found that for hot stars in cluster NGC 6705 with emission in H α line core binary model can provide fake result fitting it as a spectroscopic binary with very large $|\Delta RV| > 350 \text{ km s}^{-1}$, see Figure 3. Fortunately such results can be easily filtered out as their value $(V \sin i)_0$ hit the upper limit of the allowed range. Also observations of many stars, especially in NGC 6705, have spectral line at $\lambda = 6614 \text{ \AA}$, which is absent in our models. We suspect this is Diffuse Interstellar Band (van Loon et al. 2013), as some clusters are located close to the Milky Way plane. Fortunately absence of this line in our spectral models have no effect to our selection as both single-star and binary model have been affected in similar way.

The criteria outlined above are used to select binary candidates after spectral analysis. In total 60 SB2 candidates are selected: two in NGC 2243, eight in NGC 2420 and NGC 3532, 17 in NGC 6253 and 25 in NGC 6705, see Tables A1 and A2. Figure 4 shows the results of the selection. The selected SB2 candidates (black open triangles) fall below the blue dashed line as per the selection criteria. Known SB candidates from the literature are also highlighted. Among selected sample of 60 SB2 candidates, 18 were previously reported as spectroscopic binaries, which means that we identified 42 new ones. In comparison with our results for synthetic stars we have much smaller number of selected stars with big $(V \sin i)_0$, which means that the radial velocity separation was smaller in comparison with mock binaries. Similarly to simulations, an overdensity parallel to the blue line (in the range $50 < (V \sin i)_0 < 200 \text{ km s}^{-1}$) is also visible in our results. This is highly likely single stars. We found a relatively small number of SB2s in many clusters, which can be due to selection strategy of Gaia-ESO survey (Bragaglia et al. 2022), which was not focused on the detection of spectral binaries (Merle et al. 2020).

Our selection finds only five SB2 candidates from 26 reported in Kovalev & Straumit (2022), where selection was based on visual inspection of the plots and improvement factor. Many not selected SB2s contain two fast rotating stars, so our criterion can select them only for a very big radial velocity separation.

Figure 5 shows examples of the fitting for three SB2 candidates. Visual inspection of the selected spectra confirms two spectral components, thus our criterion works well. However we should note, that all these SB2 candidates must be confirmed by additional spectral observations, as they can be result of chance alignment, which is more likely in stellar clusters due to crowding.

Three of the selected SB2 candidates, 16590077-5241368 and 16592336-5242335 from NGC 6253 and 11031396-5828578 from NGC 3532, are previously reported as SB1s in Merle et al. (2020) and non-single stars orbit catalogue Gaia Collaboration et al. (2022). Since two spectral components are evident in the spectra (see Figure 6), these systems should be reconsidered as SB2 candidates.

The two eclipsing binaries in NGC 3532, HD 96609 (11065791-5841574) and HD 303734 (11032541-5830001), described by Özdarcın (2022), were included in the present analysis. However, their spectra were not selected by the method as SB2 candidates. The spectra, depicted in Figure 7, show that the binary fit does not significantly improve upon the single star model. It is possible that these spectra were observed, when the stars were in the part of their orbits where they had no radial velocity discrepancy.

The implementation of this method has found several limitations. First, stars with temperatures that are lower or higher than the range of the grid used in the model lead to high errors in the spectral fitting. Specifically, the model could not account for spectral lines profiles of the hot stars ($T_{\text{eff}} > 8700 \text{ K}$) that exceeded the range of the grid, thus it could have attempted to corrected for broadening by

increasing the estimated rotational velocity $(V \sin i)_0$, which could lead to erroneous selection of single stars as SB2s. Also, very cool stars of temperatures $T_{\text{eff}} < 5000 \text{ K}$ are poorly fitted, as they can have molecular bands, absent in our models. Such fits were excluded after the visual inspection. Low S/N of the observed spectra was found to be another source of false selection. The binary components of the model fit to the noise of the spectra, producing two spectral components that may not truly appear in the observed spectra.

7 CONCLUSIONS

This paper tests the reliability of the selection criteria proposed by Kovalev et al. (2022b) to detect SB2s by applying them to five open clusters. The method for selection depends on the assumption, that a single star model compensates for the disparity of double spectral components by increasing the estimated projected rotational velocity. Analysis of both synthetic and observed datasets shows that this method is effective at selecting binaries without producing false positive selections. The method found 60 SB2 candidates overall, with 18 of them previously documented in literature. We plan to apply this selection for all available HR15N spectra in the future paper.

ACKNOWLEDGEMENTS

We are grateful to the anonymous referee for a constructive report and suggestions, which greatly improved the paper. MK is grateful to his parents, Yuri Kovalev and Yulia Kovaleva, for their full support in making this research possible. This work is supported by National Key R&D Program of China (Grant No. 2021YFA1600401/3), International Centre of Supernovae, Yunnan Key Laboratory (No. 202302AN360001) and by the Natural Science Foundation of China (Nos. 12090040/3, 12125303, 11733008). The authors gratefully acknowledge the ‘‘PHOENIX Supercomputing Platform’’ jointly operated by the Binary Population Synthesis Group and the Stellar Astrophysics Group at Yunnan Observatories, Chinese Academy of Sciences. Based on data products from observations made with ESO Telescopes at the La Silla Paranal Observatory under run IDs 079.D-0825, 188.B-3002 and 193.B-0936. This research has made use of NASA’s Astrophysics Data System, the SIMBAD data base, and the VizieR catalogue access tool, operated at CDS, Strasbourg, France. It also made use of TOPCAT, an interactive graphical viewer and editor for tabular data (Taylor 2005).

DATA AVAILABILITY

The data underlying this article will be shared on reasonable request to the corresponding author.

REFERENCES

- Bragaglia A., et al., 2022, *A&A*, **659**, A200
- Bressan A., Marigo P., Girardi L., Salasnich B., Dal Cero C., Rubele S., Nanni A., 2012, *MNRAS*, **427**, 127
- El-Badry K., Rix H.-W., Ting Y.-S., Weisz D. R., Bergemann M., Cargile P., Conroy C., Eilers A.-C., 2018a, *MNRAS*, **473**, 5043
- El-Badry K., et al., 2018b, *MNRAS*, **476**, 528
- Gaia Collaboration et al., 2022, arXiv e-prints, p. arXiv:2208.00211
- Gilmore G., et al., 2012, *The Messenger*, **147**, 25
- Grupp F., 2004a, *A&A*, **420**, 289
- Grupp F., 2004b, *A&A*, **426**, 309

- Kovalev M., 2019, PhD thesis, Heidelberg University, doi:10.11588/heidok.00027411
- Kovalev M., Straumit I., 2022, *MNRAS*, 510, 1515
- Kovalev M., Li Z., Zhang X., Li J., Chen X., Han Z., 2022a, *MNRAS*, 513, 4295
- Kovalev M., Chen X., Han Z., 2022b, *MNRAS*, 517, 356
- Kovalev M., Wang S., Chen X., Han Z., 2023, *MNRAS*, 519, 5454
- Liu C., et al., 2020, *arXiv e-prints*, p. arXiv:2005.07210
- Merle T., et al., 2017, *A&A*, 608, A95
- Merle T., et al., 2020, *A&A*, 635, A155
- Moe M., Stefano R. D., 2017, *The Astrophysical Journal Supplement Series*, 230, 15
- Özdarcan O., 2022, *MNRAS*, 509, 1912
- Pasquini L., et al., 2002, *The Messenger*, 110, 1
- Piccotti L., Docobo J. Á., Carini R., Tamazian V. S., Brocato E., Andrade M., Campo P. P., 2020, *MNRAS*, 492, 2709
- Randich S., et al., 2022, *A&A*, 666, A121
- Reetz J., 1999, PhD thesis, Ludwig-Maximilians-Universität München
- Schlesinger K. J., Johnson J. A., Lee Y. S., Masseron T., Yanny B., Rockosi C. M., Gaudi B. S., Beers T. C., 2010, *ApJ*, 719, 996
- Serenelli A., et al., 2021, *A&ARv*, 29, 4
- Taylor M. B., 2005, in Shopbell P., Britton M., Ebert R., eds, *Astronomical Society of the Pacific Conference Series Vol. 347, Astronomical Data Analysis Software and Systems XIV*. p. 29
- de Marchi F., Poretti E., Montalto M., Desidera S., Piotto G., 2010, *A&A*, 509, A17
- van Loon J. T., et al., 2013, *A&A*, 550, A108

APPENDIX A: TABLES WITH SELECTED SB2 CANDIDATES

Table A1 contains a list of selected SB2s and their object names as recorded in the ESO archive together with Gaia DR3 `source_id`. Table A2 have some additional info, like best-fit spectral parameters for the single star and the binary models. These parameters should be used with care, because they are serving just as a “best matching template”.

This paper has been typeset from a $\text{\TeX}/\text{\LaTeX}$ file prepared by the author.

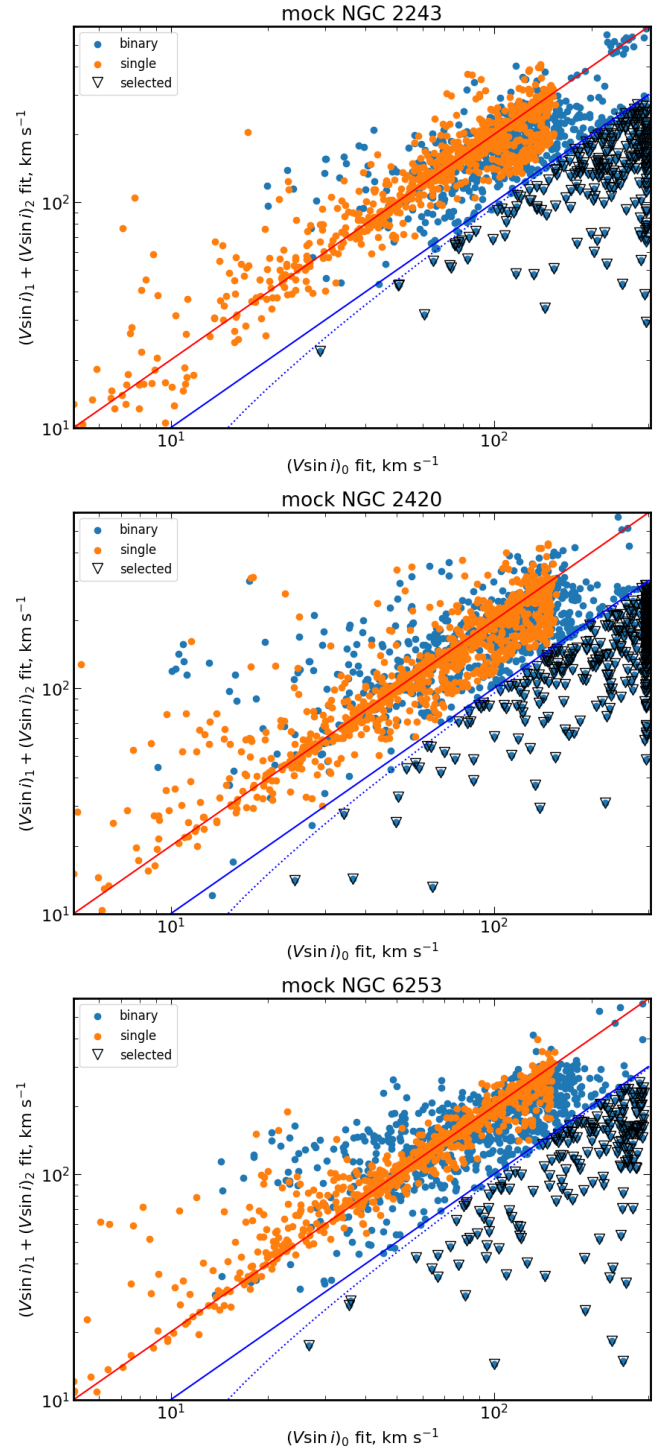


Figure 1. $(V \sin i)_1 + (V \sin i)_2$ vs. $(V \sin i)_0$ plot for synthetic stars from three clusters with $\log \text{Age}(\text{yrs}) > 9$. Blue and red lines shows relations $(V \sin i)_1 + (V \sin i)_2 = (V \sin i)_0$ and $(V \sin i)_1 + (V \sin i)_2 = 2(V \sin i)_0$ respectively. Dotted line shows relation $(V \sin i)_1 + (V \sin i)_2 + 5 = (V \sin i)_0$

Table A1. Catalogue of selected SB2 candidates. M+17 - Merle et al. (2017), M+20 - Merle et al. (2020), KS22 - Kovalev & Straumit (2022), GDR3 - Gaia Collaboration et al. (2022).

Cluster	ESO cname	GDR3 source_id	G, mag	remark
NGC 2243	06290412-3114343	2893945772888126720	14.934553	SB2 M+17
NGC 2243	06292643-3115445	2893942921030310912	16.304037	
NGC 2420	07374440+2136232	865412923480423680	17.150282	
NGC 2420	07380618+2137236	865402860372744704	15.4575	
NGC 2420	07382246+2132287	865399939794989952	15.667797	
NGC 2420	07382338+2131396	865396950497755264	16.9582	
NGC 2420	07382366+2133430	865401485983205504	15.800236	
NGC 2420	07383323+2135213	865401657781870080	15.149413	
NGC 2420	07384133+2134225	865398939066030976	16.65745	
NGC 2420	07384553+2129385	865397122296423424	14.6743	
NGC 3532	11020707-5855342	5338686027293771904	17.397034	
NGC 3532	11022934-5845476	5338682934919078784	17.219435	
NGC 3532	11024689-5844177	5338706299537601280	11.168904	
NGC 3532	11030296-5900435	5338675758080306816	12.7284046	astrometric acceleration GDR3
NGC 3532	11031396-5828578	5338715782825370368	12.163282	SB1 GDR3
NGC 3532	11054586-5857236	5338651225224549632	17.295105	
NGC 3532	11065099-5838199	5340161576236734848	11.287692	
NGC 3532	11073165-5848233	5340147729260314752	15.834448	
NGC 6253	16583965-5235499	5935994452129297152	14.892061	
NGC 6253	16584301-5247576	5935967136135123840	14.236232	
NGC 6253	16585321-5242431	5935991291033271168	14.035797	
NGC 6253	16585749-5242259	5935944389986065408	14.101318	
NGC 6253	16590035-5245080	5935944183827814016	14.592207	
NGC 6253	16590077-5241368	5935945897460206080	14.928719	SB1 M+20
NGC 6253	16590417-5237044	5935993524416300800	16.764376	
NGC 6253	16590446-5240362	5935946039253519232	14.361807	
NGC 6253	16590609-5242566	5935945798735308160	14.448471	
NGC 6253	16590624-5242009	5935945833095064192	14.367528	
NGC 6253	16590845-5240439	5935945970534033408	14.527414	
NGC 6253	16591059-5242177	5935945936174263040	14.72464	
NGC 6253	16591586-5245025	5935944046388593408	14.932591	
NGC 6253	16591656-5244053	5935945523857356800	14.223827	
NGC 6253	16591716-5242442	5935945661296332032	14.544811	
NGC 6253	16592297-5235100	5935952735057641856	16.270937	
NGC 6253	16592336-5242335	5935945695656057216	14.746293	SB1 M+20
NGC 6705	18502379-0615209	4252509585784232576	16.581614	
NGC 6705	18503230-0617112	4252509246592782464	13.291144	SB2 M+17
NGC 6705	18503690-0621100	4252496636566974592	16.33684	SB2 M+17
NGC 6705	18503840-0617048	4252497525515917440	16.362226	SB2 M+17
NGC 6705	18504183-0623464	4252495502695435776	15.965503	
NGC 6705	18504188-0622567	4252495605774692096	16.201315	
NGC 6705	18504222-0607490	4252518798601477504	15.961194	
NGC 6705	18504649-0611443	4252516118541710336	15.716564	SB2 M+17
NGC 6705	18504896-0614324	4252503955192670080	15.743275	
NGC 6705	18505045-0617310	4252503096165723776	18.395308	
NGC 6705	18505561-0614552	4252503920832494464	16.174961	SB2 M+17
NGC 6705	18505701-0615044	4252503710273899264	15.850019	
NGC 6705	18505726-0609408	4252517767809140864	16.413301	
NGC 6705	18505933-0622051	4252493131873385600	16.42047	SB2 M+17
NGC 6705	18510072-0609118	4252517802168868352	16.614513	SB2 M+17
NGC 6705	18510286-0615250	4252503744633664640	13.157031	SB2 M+17
NGC 6705	18510288-0617400	4252502786927640960	17.8157	
NGC 6705	18510456-0617121	4252502782561000704	12.734941	SB2 M+17
NGC 6705	18511131-0617491	4252502546409177856	17.137434	
NGC 6705	18511134-0616106	4252502919999990528	13.862979	SB2 M+17
NGC 6705	18511220-0617467	4252502542042872192	15.212772	SB2 M+17
NGC 6705	18511434-0617090	4252502645122095232	16.732573	SB2 M+17
NGC 6705	18512031-0609011	4252506218523086080	12.372231	SB2 KS22
NGC 6705	18512604-0610504	4252505943652338432	15.581753	
NGC 6705	18513193-0612518	4252504814185976960	16.381422	SB2 M+17

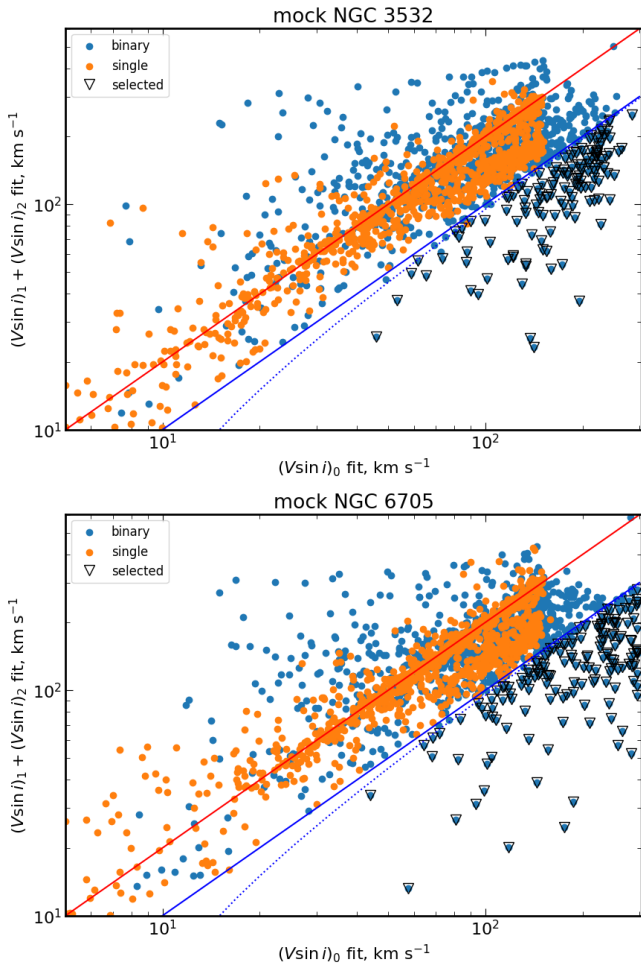


Figure 2. Same as Fig. 1 for synthetic stars from two clusters with $\log \text{Age}(\text{yrs}) < 9$.

Table A2. Additional information for selected SB2 candidates. Full table is available online as a supplemental material.

parameter	unit
ESO cname	
$T_{\text{eff}0}$	K
$\log(g)_0$	dex
$[\text{Fe}/\text{H}]_0$	dex
$(V \sin i)_0$	km s^{-1}
$T_{\text{eff}2}$	K
$\log(g)_2$	dex
$[\text{Fe}/\text{H}]_{1,2}$	dex
$(V \sin i)_2$	km s^{-1}
$T_{\text{eff}1}$	K
$\log(g)_1$	dex
$(V \sin i)_1$	km s^{-1}
RV_0	km s^{-1}
RV_2	km s^{-1}
RV_1	km s^{-1}
q	
imp	
S/N	pix^{-1}
MJD	d
GDR3 source id	
G	mag

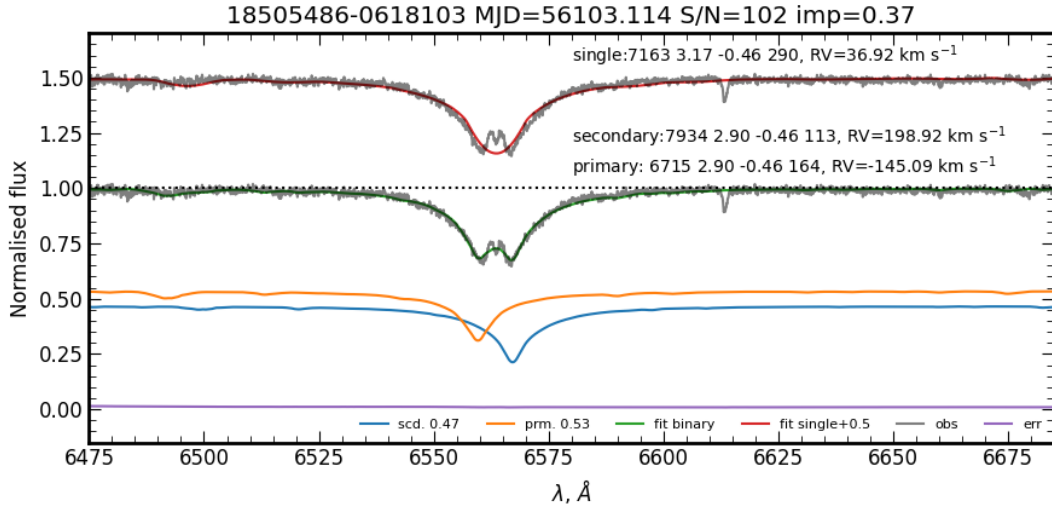


Figure 3. Examples of spectral fits with single-star and binary models for hot star with emission in $H\alpha$ line core. This star was falsely selected as SB2 candidate, but can be easily eliminated thanks to the criterion on the large $(V \sin i)_0$. Titles shows modified julian date (MJD), signal to noise ratio and improvement factor. Best-fit spectral parameters (RV , T_{eff} , $\log(g)$, $[\text{Fe}/\text{H}]$, $(V \sin i)$) are given for all fits.

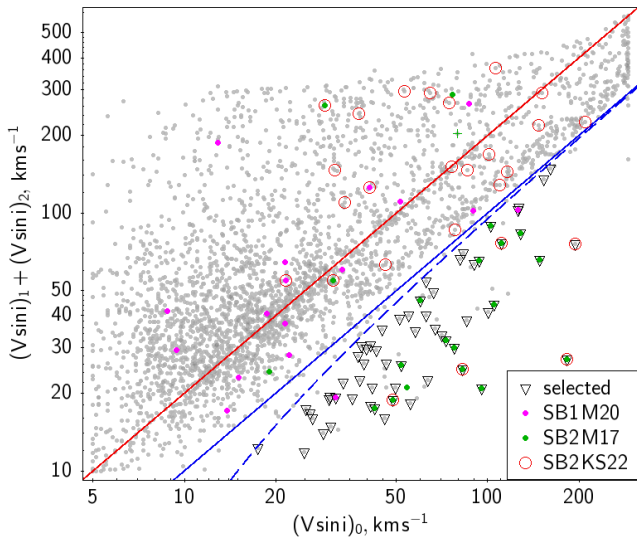


Figure 4. Same as Fig. 1 for all observed spectra from five clusters. Selected SB2 candidates are shown as black open triangles. Known SB candidates are also highlighted.

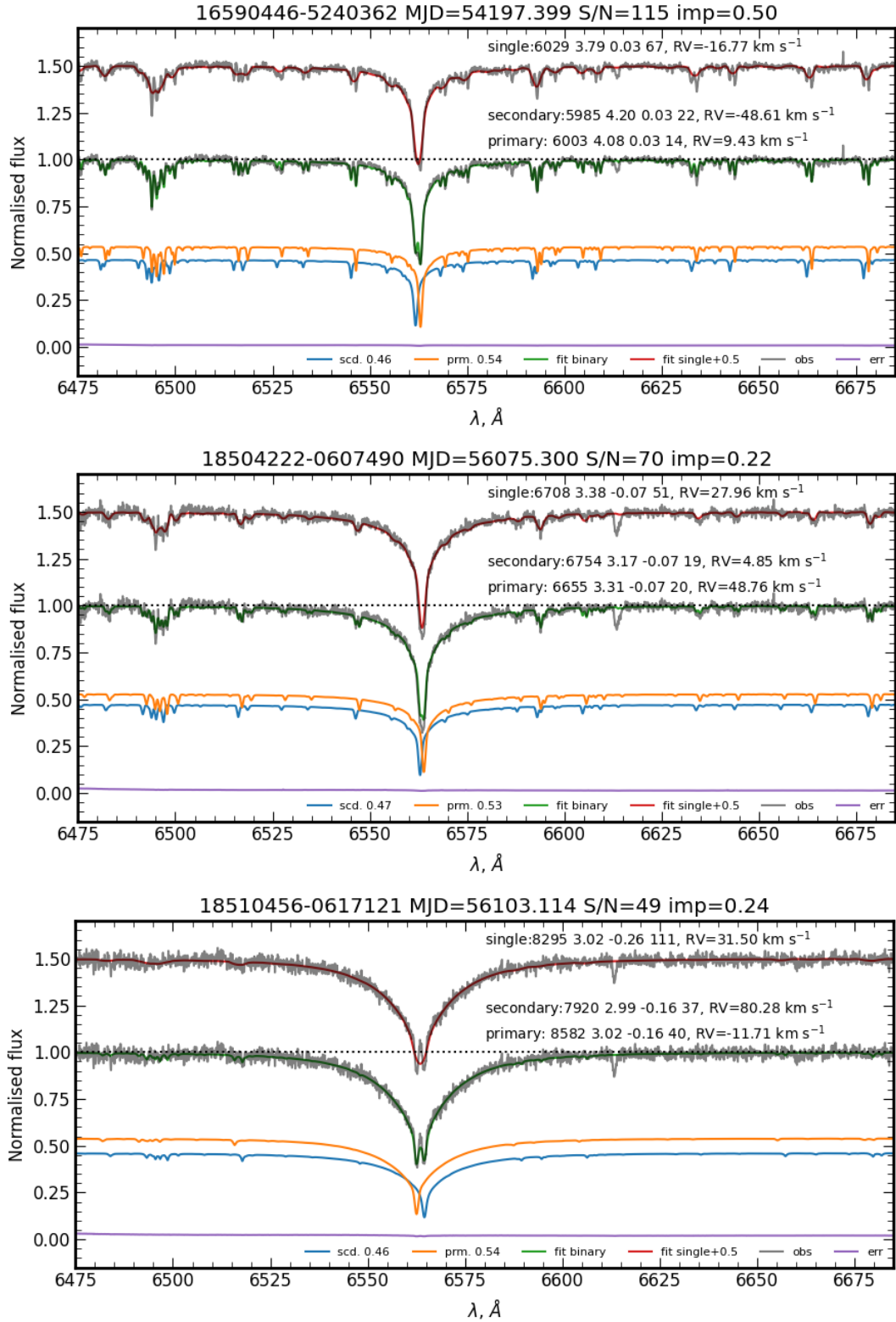


Figure 5. Same as Fig. 3 for three SB2 candidates

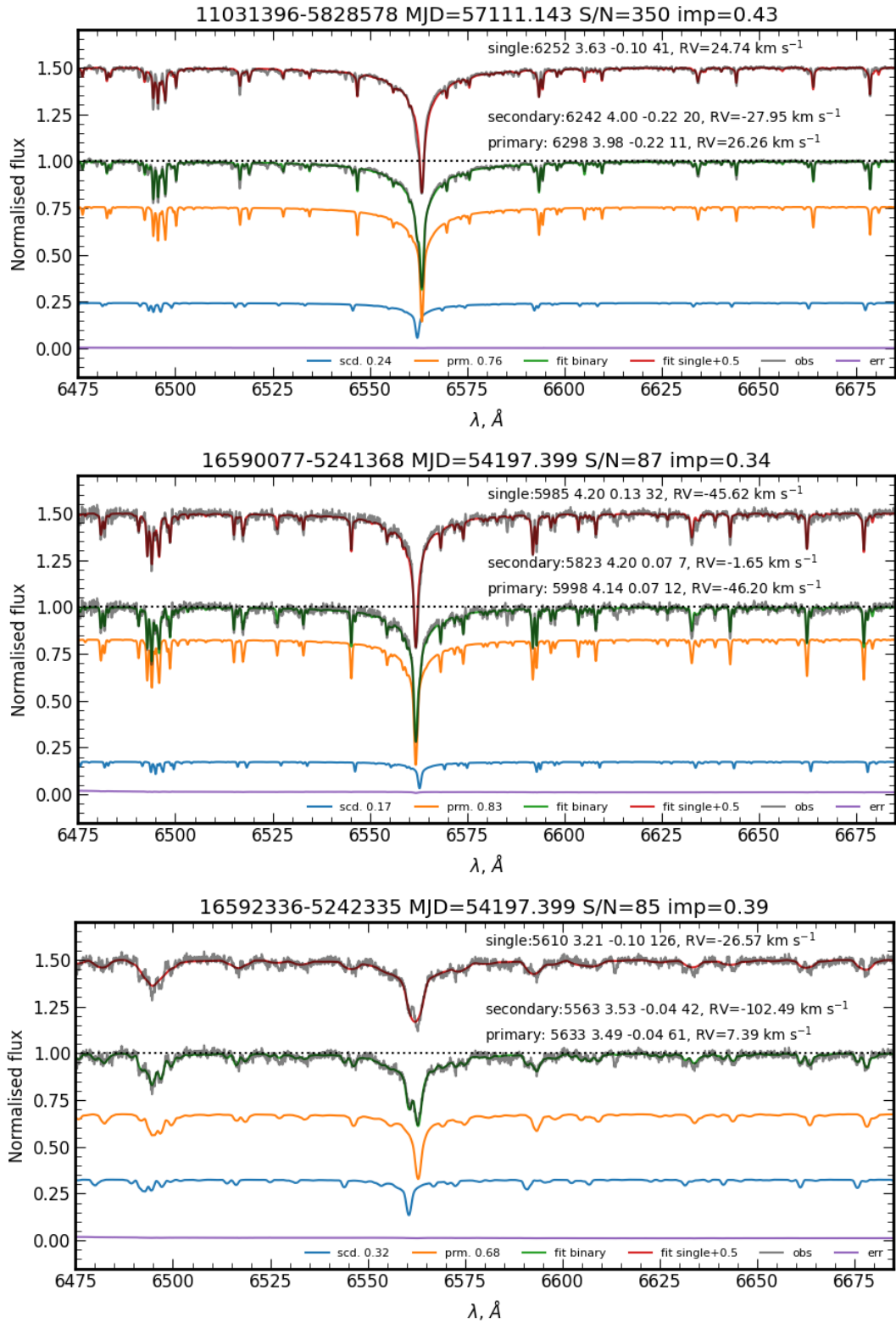


Figure 6. Same as Fig. 3 for three SB2 candidates, previously reported as SB1.

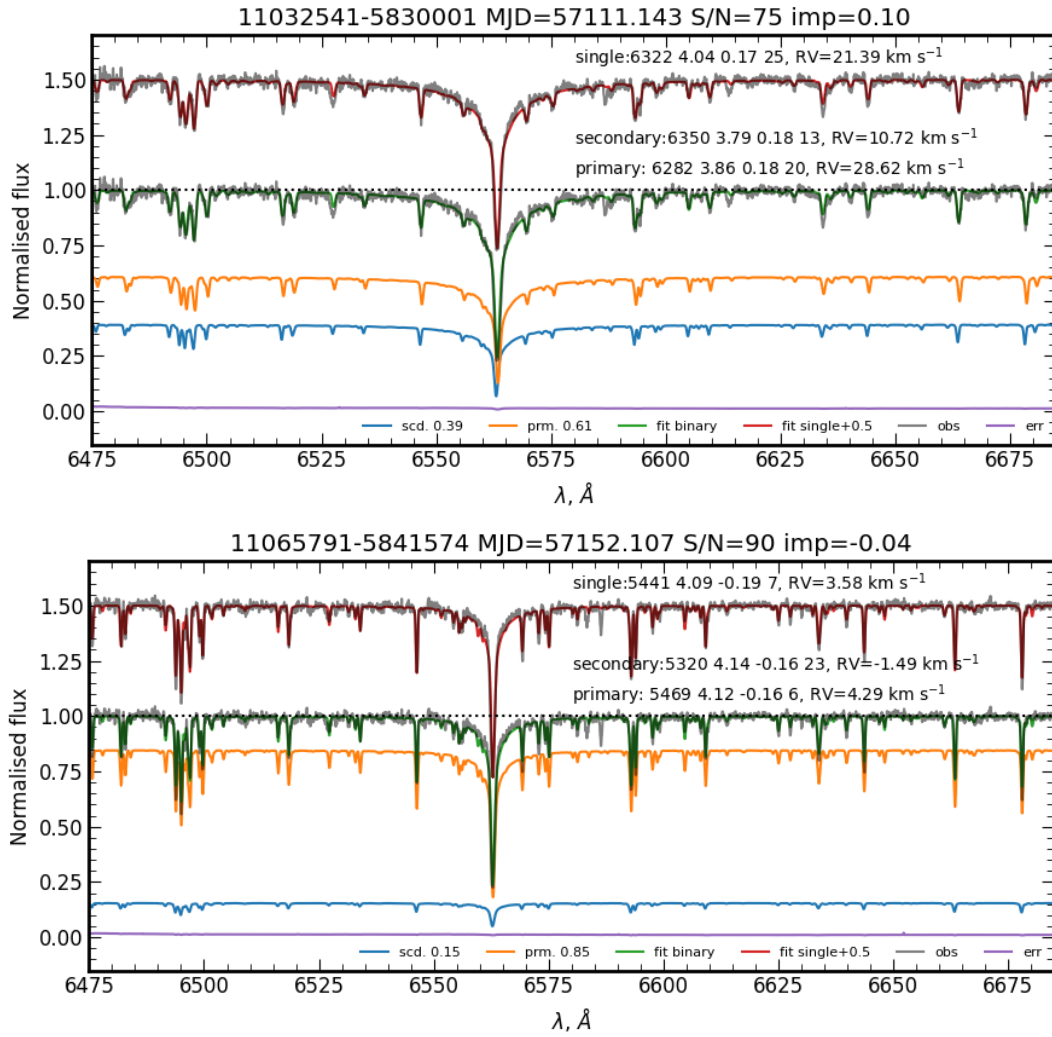


Figure 7. Same as Fig. 3 for two known eclipsing binaries from NGC 3532: HD 96609 (top) and HD 303734 (bottom), but not selected as SB2 by our method because the binary models do not significantly improved the fit over the single star models.